Chemical Papers (2021) 75:4949–4958
https://doi.org/10.1007/s11696-021-01715-7

ORIGINAL PAPER

Ruthenium (III)–pyridine complex: Synthesis, characterization, barrier diode and photodiode applications in Al/Ru-Py/p-Si/Al sandwich device structure

Ali Yeşildağ[1]

Received: 26 January 2021 / Accepted: 21 May 2021 / Published online: 1 June 2021

Abstract
Ruthenium (III)–pyridine (Ru-Py) complex has been synthesized and characterized by NMR, IR, UV–Vis, fluorescence spectroscopy and HRMS. The crystal structure of the Ru-Py complex was determined by X-ray crystallography. The Ru-Py complex was coated on a p-type Si semiconductor by a spin coating method to obtain a Schottky barrier diode (SBD) device. Basic electrical parameters of the obtained Al/p-Si/Al MS and Al/Ru-Py/p-Si/Al SBD devices were calculated by using thermionic emission (TE) theory such as ideality factor (n) and barrier height (Φ_b). From the current–voltage (I–V) measurements, the n value of the reference Al/p-Si/Al MS structure was 1.55 and the Al/Ru-Py/p-Si/Al SBD structure was 1.24 at room temperature. The Ru-Py complex as interface material made the device behave more ideally and decreased the value of the ideality factor. Φb values of the reference MS and SBD devices were calculated as 0.67 and 0.78 eV, respectively. The presence of Ru-Py complex films in the device structure increased the barrier height. Additionally, using the C^{-2}–V graph obtained from frequency-dependent C–V measurements, the diffusion potential (V_d), acceptor concentration (N_a), Fermi energy (E_f), barrier height (Φ_b) parameters of Al/Ru-Py/p-Si/Al device were calculated. Current–voltage (I–V) measurements of the device obtained with Ru-Py complex were taken in different lighting intensity. In the I–V characteristics, the reverse and forward bias current increased depending on the light. It was concluded that the Al/Ru-Py/p-Si/Al device is suitable for photodiode applications.

Keywords Ruthenium (III)–pyridine complex · Schottky barrier diode · Photodiode · Electrical characterization

Introduction

The working principle of most electronic and optoelectronic devices used today is based on metal–semiconductor (MS) contact structure with a rectifier feature. Depending on the vacuum technology developed in recent years, the production of Schottky barrier diodes has become easier (Taşyürek et al. 2018; Çaldiran 2020). Among the areas in which MS contacts are used, there are many electronic applications such as Schottky solar cells based on thin films (Chen et al. 2012), photodetectors (Ravikiran et al. 2016), gas sensors (Punetha and Pandey 2019), field-effect transistors (FET) (Di Bartolomeo et al. 2018), photodiodes (Koçyiğit et al. 2017), organic light-emitting diodes (OLED) (Gao et al. 2016) and photocatalysis (Petronella et al. 2011). In these applications, Schottky barrier height (SBH) is known as important for rectifier contacts. Since the increasing SBH strengthens the rectifier character, the researches have been carried out using different semiconductors and metals (Çaldıran et al. 2013a, b; Ejderha et al. 2011; Reddy and Choi 2020). Organic materials (Gupta and Singh 2004; Ahmad and Sayyad 2009), insulators (Altındal et al. 2006; Güllü and Türüt 2015), nanomaterials (Park et al. 2003; Yılmaz et al. 2018), oxide materials (Djeghlouf et al. 2019; Metin et al. 2014; Tuğluoğlu et al. 2005) or organometallic materials are used as the interface in the MS contact structure to raise the SBH. Additionally, a positive effect is reported on the performance by facilitating the adjustment of SBH in heterojunction structures formed between two different semiconductors (Coşkun et al. 2019; Izaki et al. 2007; Taşyürek et al. 2020).

✉ Ali Yeşildağ
aliyesildag@yahoo.com

[1] Department of Bioengineering, Faculty of Engineering and Architecture, Kafkas University, Kars, Turkey

Researches on electronic and optoelectronic devices fabricated by the modification of various films such as organic, inorganic and organometallic thin films as materials between semiconductor and metal have attracted attention in recent years (Farag et al. 2010; Karabulut et al. 2018; Dragonetti et al. 2013) since the thin-film materials used between semiconductor and metal can provide the fabrication of devices with desirable characteristics such as electrical and optical properties. The organometallic film materials used particularly as interfacial layers have great importance because they are of interest due to their versatile the photochemical, photophysical and electrochemical properties. These properties strongly depend on the oxidation states of the metal used in the organometallic complexes. One of the various organometallic film materials is ruthenium complexes. The ruthenium complexes have gained interest in the preparation of organometallic complexes for multiple applications in many fields like FET, OLED and photovoltaic. Up to now, many studies have been reported on the preparation of Ru (II) complexes for photochemical and photophysical applications (Juris et al. 1988; Sauvage et al. 1994; Vergeer et al. 2006; Zhang et al. 2007). However, the spectroscopic and electrochemical properties of Ru (III) complexes are still not clear (Lakshmanan et al. 2018; Benavides et al. 2017; Kar et al. 2017; Białek and Latos-Grażyński 2016; Alessio et al. 1991). The photochemical, photophysical and redox properties of Ru (III) complexes are of great interest among the researchers for their range of fundamental and practical applications (Benavides et al. 2017; Chmielewski et al. 1994; Alessio et al. 1991; Latos-Grazynski et al 1989). They exhibit a strong emission and these emission bands could be due to the MLCT process of the complexes (Lakshmanan et al. 2018; Kar et al. 2017; Białek and Latos-Grażyński 2016; Taqui Khan et al. 1993; Mohita et al. 2020; Umamahesh et al. 2016).

For the devices, I–V measurements can be made at room temperature to make the electrical characterization of SBDs. The semi-logarithmic I–V characteristic can give information about the contact structure. In the literature, many studies on the SBD interface states have been published (Ejderha et al. 2011), (Altındal et al. 2006). Photodiode behavior can be evaluated by making I–V measurements in the dark and under different illuminations (Orak et al. 2017). Moreover, capacitance–voltage (C–V) measurements give more detailed information about the SBD structure and charge carriers.

In the present study, the Ru-Py complex materials were synthesized in high yield and spectroscopically characterized. Later, Al/Ru-Py/p-Si/Al SBDs with electrical and photo-responsive properties were obtained by forming an ultra-thin-film Ru-Py complex interface using spin coating method on p-type Si. Using thermionic emission (TE) theory at room temperature, parameters such as barrier height (Φ_b), ideality factor (n) and series resistance (R_s) from semi-logarithmic I–V characteristics were calculated. Its photodiode properties were determined by examining semi-logarithmic I–V measurements in dark and illumination. Besides, the other parameters such as Fermi energy level, diffusion potential, carrier concentration and barrier height were calculated by using current–voltage measurements.

Experimental

Synthesis of Ru-Py complex

In 6 mL of pure ethanol and 6 mL of 1 N HCl was dissolved 1 mmol $RuCl_3.H_2O$ and refluxed for 3 hour. The mixture was cooled at room temperature. Then, 6 mmol of pyridine was dissolved in 2 mL of ethanol and 1 mL of 6 N HCl, and it was added while stirring the mixture. The last mixture was stirred for about 45 min at 30 °C. Then, the last mixture was left for 3 days at room temperature. The dark brown crystals were filtered off, washed with ethanol and ether and dried in vacuo. Yield: (85%). Anal. Calcd for $C_{15}Cl_4H_{16}N_3Ru$ (M) 481.2): Mp: 320-322 °C, ^{1}H NMR (400 MHz, DMSO) δ 9.02 (bs, 2H), 8.62 (bs, 1H), 8.09 (bs, 2H) (Fig.S1 in the Supporting İnformation). ^{13}C NMR (100 MHz, DMSO) δ 148.10, 145.09, 129.00, 95.18 (Fig. S2 in the Supporting İnformation). IR (cm^{-1}): 3213, 3154, 3129, 3100, 3063, 2961, 1632, 1603, 1533, 1482, 1450, 1442, 1359, 1330, 1233, 1212, 1157, 1064, 1048, 981, 895, 765, 744, 693, 673, 607, 575, 532, 522 cm^{-1}. HRMS (Q-TOF): m/z $[M+H-C_5H_6N]^+$ calcd. for $C_{15}H_{16}{}^{35,37}Cl_4N_3Ru$: 402.86903 (100.0%), 400.87198 (78.2%), 404.87011 (59.0%), 401.87027 (54.1%), 404.86608 (47.9%), 402.87306 (46.2%), 399.87322 (42.3%), 399.87062 (40.4%), 400.86890 (39.9%), 397.87357 (31.6%), 398.87185 (31.2%), 406.86716 (28.3%), 403.86732 (25.9%), 401.86767 (19.4%), 402.86595 (19.1%), 396.87228 (17.6%), 394.87523 (13.7%), 403.87239 (10.8%); found: 402.88583, 403.88414, 404.88438, 405.88363, 406.8827, 407.88261, 408.88313, 409.88094.

X-ray diffraction analysis

A+78ASuitable crystals of Ru-Py complex were selected for data collection which was performed on a D8-Venture diffractometer equipped with a graphite-monochromatized MoK_α radiation at T = 296 K. The structures were solved by direct methods using SHELXS-97 (Sheldrick 2008) and refined by full-matrix least-squares methods on F^2 using SHELXL-2013 (Sheldrick 2015). All non-hydrogen atoms were refined anisotropically. The H atoms were located from different maps and then treated as riding atoms with C–H distances of 0.93 Å and N–H distances of 0.86 Å. The N3 and C11 atoms in the pyridine molecule are located on

a center of symmetry and are caused by the symmetrical disorder. The following procedures were implemented in our analysis: data collection: Bruker APEX2; a program used for molecular graphics were as follows: MERCURY programs; software used to prepare material for publication: WinGX (Farrugia 1999). Details of data collection and crystal structure determinations are given in Table 1.

Table 1 Crystal data and structure refinement parameters for Ru-Py complex

Empirical formula	$C_{15}H_{16}N_3Cl_4Ru$
Formula weight	481.18
Crystal system	Orthorhombic
Space group	Pnma
a (Å)	15.961 (6)
b (Å)	13.667 (6)
c (Å)	8.372 (3)
V (Å^3)	1826.1 (12)
Z	4
D_c (g cm^{-3})	1.750
θ range (º)	3.1–28.2
Measured refls.	24161
Independent refls.	2343
R_{int}	0.034
S	1.07
R1/wR2	0.021/0.047
$\Delta\rho_{max}/\Delta\rho_{min}$ (eÅ^{-3})	0.55/−0.36

Preparation of junction diode

The cleaning procedure used to clean the p-type Si first in the production stages of the device was performed as in the study reported by Taşyürek et al. (2018). For Ohmic back contact, Al metal was coated on p-type Si by thermal evaporation method at 1 Å/S in a vacuum (10^{-7} Torr). Subsequently, the Ru-Py material was coated on the other surface of the p-type Si by spin coating method at 2000 rpm for 50 seconds and annealed in a hot plate device at 120 °C for 3 minutes. Later, Al dot contacts were coated on Ru-Py by thermal evaporation method and Al/Ru-Py/p-Si/Al SBD was produced. The Al/Ru-Py/p-Si/Al device structure and measurement system are shown in Fig. 1. I–V and C–V measurements of the devices were taken at room temperature.

Instrumentation

^{1}H and ^{13}C NMR spectra were recorded on a Varian-400 and a Bruker-400 spectrometer. Mass spectra were recorded on an Agilent Technologies 6530 Accurate-Mass Q-TOF-LC/MS. Fourier transform IR spectra analyses of samples were recorded on PerkinElmer Frontier FT-IR spectrometer. Absorption measurements were taken using a PerkinElmer Lambda 35 spectrophotometer. Fluorescence spectra were taken with a Shimadzu RF5300 PC spectrofluorometer. Fluorescence lifetimes were measured by Horiba-Jobin-Yvon-SPEX Fluorolog 3–2iHR with Fluoro Hub- B. Single photon counting controller (France) was used when excitation of samples carried out with 310 nm nanoLED (France) and photon signals was obtained via TCSPC module. X-ray data

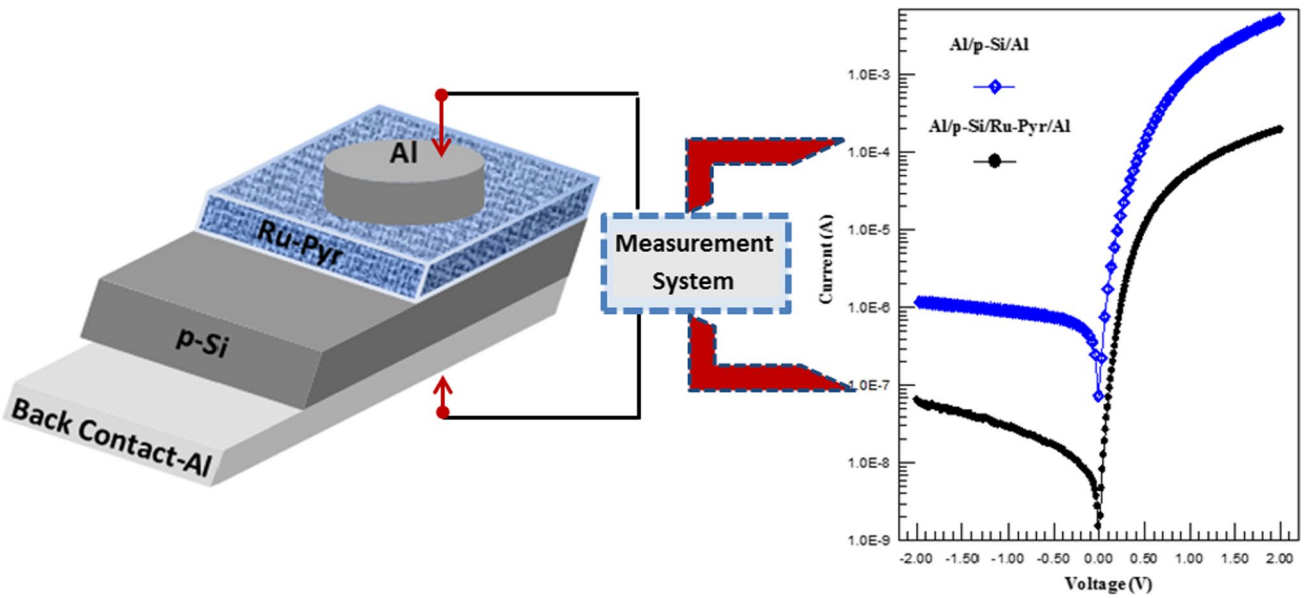

Fig. 1 Schematic representation of the measurement system and the fabricated Al/Ru-Py/p-Si/Al device

were measured by using Bruker D8 Venture diffractometers. I–V and C–V measurements of the devices were taken with Keithley 2400 Source meter at room temperature and HP 4192A (50−13 MHz) LF impedance analyzer, respectively.

Result and discussion

Characterization of Ru-Py complex

The Ru-Py complex has been successfully synthesized and found to crystallize in space group Pnma, with a = 15.961 (6), b = 13.667 (6), c = 8.372 (3) Å, and Z = 4. The molecular structure of the Ru-Py complex is shown in Fig. 2 with the atom numbering scheme. The Ru (III) ion is located on the inversion center and coordinated to two nitrogen atoms of the pyridine rings *trans* to each other and four coplanar chlorine atoms, thus showing a distorted octahedral coordination geometry. The asymmetric unit of Ru-Py complex consists of one Ru (III) ion, one and a half coordinated pyridine ligands, two chlorine atoms and half non-coordinated pyridine molecule which is a protonated and electrostatically bound to the negatively charged Ru (III) complex. An alternative synthesis of the Ru-Py complex and its characterization are described in the other two works (Batista et al. 1997; Webb et al. 2013). The crystal structure determinations and details of data collection are given in Table 1.

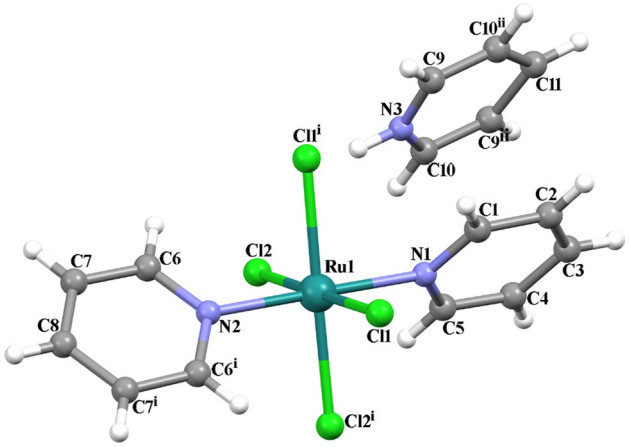

Fig. 2 The molecular structure of Ru-Py complex showing the atom numbering scheme. [(i) x,−y+1/2, z; (ii) −x+1, −y, −z+2.]

The IR spectrum of the Ru-Py complex (Fig. S3) exhibited characteristic absorptions bands for aromatic C-H, aromatic C=C, and aromatic C-N bonds. In the IR spectrum of the Ru-Py complex, the absorption bands at 2961, 3063 and 3100 cm^{-1} are attributed to aromatic C–H bonding vibrations. High-resolution mass spectrometry (HRMS) confirmed the constitution of the Ru-Py complex (Fig. S4). The HRMS results showed that the calculated mass was consistent with the mass obtained. There are 35 and 37 isotopes of the chlorine atoms in the complex. Therefore, isotope peaks of 4 chlorine atoms are also seen in the HRMS spectrum (see Experimental section).

Fig.3a shows the UV/Vis spectra of the Ru-Py complex. The first peak is observed at λ = 259 nm and is assigned to the autochrome signal from the pyridine ligand (Siek and Osiewicz 1975). The second absorbance peak occurs at λ=315 nm, which is consistent with pyridine π–π^* transitions for the Ru-Py complex (Manoharan et al. 1973). The other peak at λ=376 nm is shown the typical range of ligand-to-metal charge-transfer (LMCT) transitions with

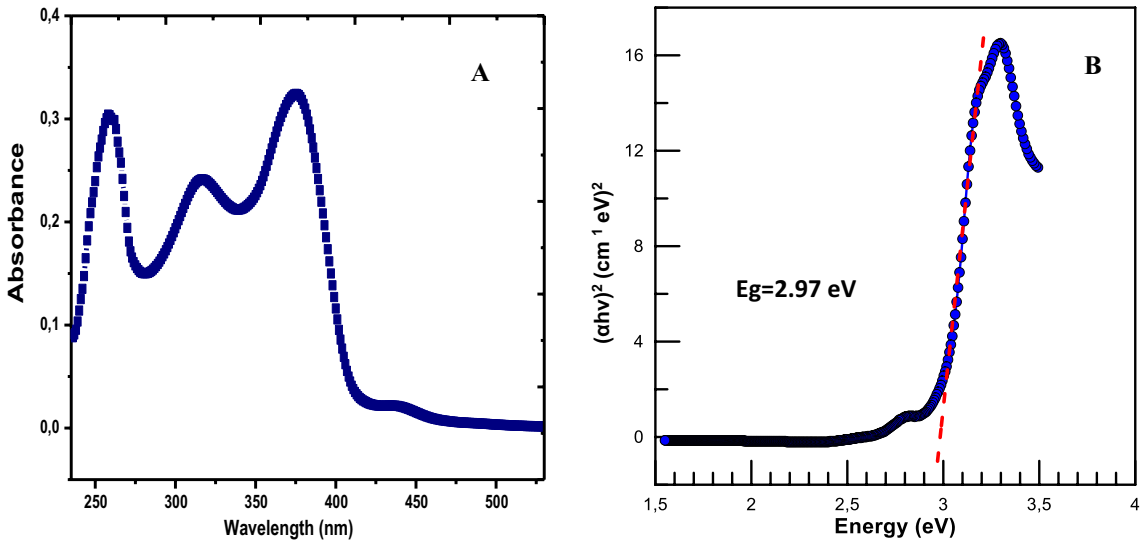

Fig. 3 UV/Vis spectra (**a**) and graph of (hν)1/2 versus (hν) (**b**) for Ru-Py complex in DMSO

bound nitrogen for Ru-Py complex (Kroghjespersen and Schugar 1984)

UV–Vis absorption spectroscopy is used to determine the optical band gap (E_g) of the Ru-Py complex film. Figure 3b shows the optical absorption spectrum as a function of the energy of the Ru-Py complex film coated on the glass substrate. The band gap of the thin organometallic film can be determined using the Tauc equation given below (Orhan et al. 2020).

$$ah\nu = A\left(h\nu - E_g\right)^n \quad (1)$$

where α is used as the absorption coefficient, hν is used as the energy of the incident photon, and A is used as constant. The optical band gap of the Ru-Py complex was determined from the graph of $(\alpha h\nu)^2$ versus hν and using the Tauc equation. The intersection point of the graph gives the value of the optical band gap and is determined as 2.97 eV for the Ru-Py complex.

Its fluorescence property was examined by using steady-state and time-resolved fluorescence measurements. The fluorescence spectrum of the Ru-Py complex in DMSO was recorded with an excitation wavelength of 340 nm at room temperature (c = 5 μM) (Fig. 4). From the figure, the Ru-Py complex showed one fluorescence band in the visible region and its maximum was found at 411 nm. To determine the fluorescence lifetime of the Ru (III)-Py complex, its fluorescence decay was taken with 310 nm of excitation wavelength and fitted (Fig. S5). The fluorescence lifetime value was calculated as 26 ns. The lifetime value supported the fluorescence property of the Ru-Py complex (Lakshmanan et al. 2018; Benavides et al. 2017; Kar et al. 2017; Białek and Latos-Grażyński 2016; Chmielewski et al. 1994; Alessio et al. 1991). It can be concluded that the Ru-Py complex can be used as a promising material in different optoelectronic technologies such as OLEDs and photovoltaic (Fig. 5).

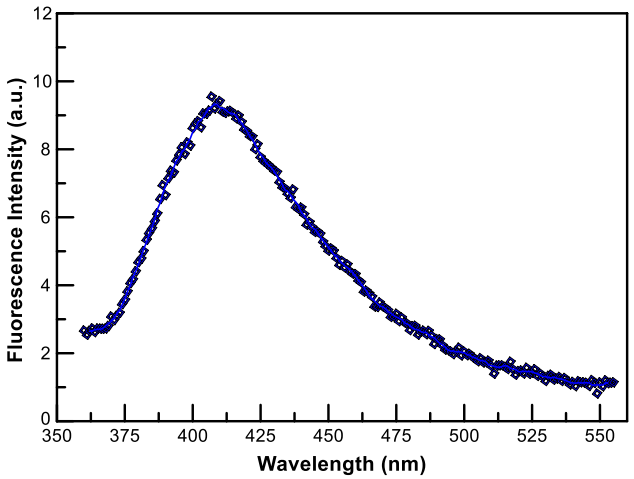

Fig. 4 Fluorescence emission spectra for Ru-Py complex

Current–voltage (I–V) characteristics

The semi-logarithmic I–V characteristics of the SBDs in forwarding bias are expressed by the TE method with the following equation (Tung 2001);

$$[I = ART^2 \exp\left(-\frac{q\Phi_b}{kT}\right)\left[\exp\left(\frac{qV}{nkT} - 1\right)\right] = I_0\left[\exp\left(\frac{qV}{nkT} - 1\right)\right] \quad (2)$$

is the area and its size is 7.85×10^{-3} cm^2, R is the Richardson constant of the semiconductor, T is the temperature, q is the electronic charge, Φ_b is the barrier height, k is the Boltzmann constant, V is the voltage, and n is the unitless ideality factor. The value of n is unique for ideal devices. The intersection point of the semi-logarithmic I–V curve with the vertical axis gives the saturation current (I_0) value.

$$I_0 = AA^*T^2 \exp\left(\frac{q\Phi_b}{kT} - 1\right) \quad (3)$$

ideality factor is obtained Eq. 2;

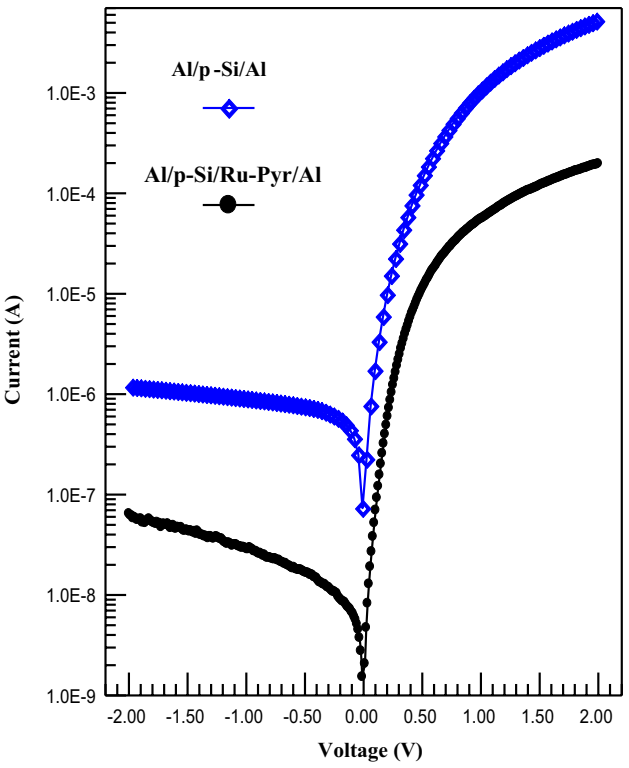

Fig. 5 The semi-logarithmic I–V characteristics of the reference diode and the Al/Ru-Py/p-Si/Al junction diode

$$n = \frac{q}{kT}\frac{dV}{d(\ln I)} \tag{4}$$

Also, Φ_b is found from Eq. 4 as:

$$\Phi_b = \frac{kT}{q}\ln\left(\frac{ART^2}{I_0}\right) \tag{5}$$

In Fig. 6, semi-logarithmic I–V plots of reference Al/p-Si/Al MS and Al/Ru-Py/p-Si/Al SBD at room temperature are given. The rectifier characteristic was observed in both device structures and leakage currents occurred in reverse bias (Kacus et al. 2014). When the forward and reverse bias currents were examined, it was observed that the rectification rate of the device obtained with Ru-Py complex was higher (Taşer et al. 2017). In forward bias in the I–V characteristic of Al/Ru-Py/p-Si/Al device, the current increased as a linear low voltage and the current value was decreased because of the effect of R_s at high voltage values (0.5 V). This behavior is quite compatible with literature studies (Taşyürek et al. 2020; Deniz et al. 2018). The n and Φ_b values calculated by the TE method in the linear region of the forward bias are shown in Table 2.

The barrier height values of the Al/p-Si/Al MS and Al/Ru-Py/p-Si/Al SBD were calculated as 0.67 eV and 0.78 eV, respectively. Accordingly, the ideality factor values of

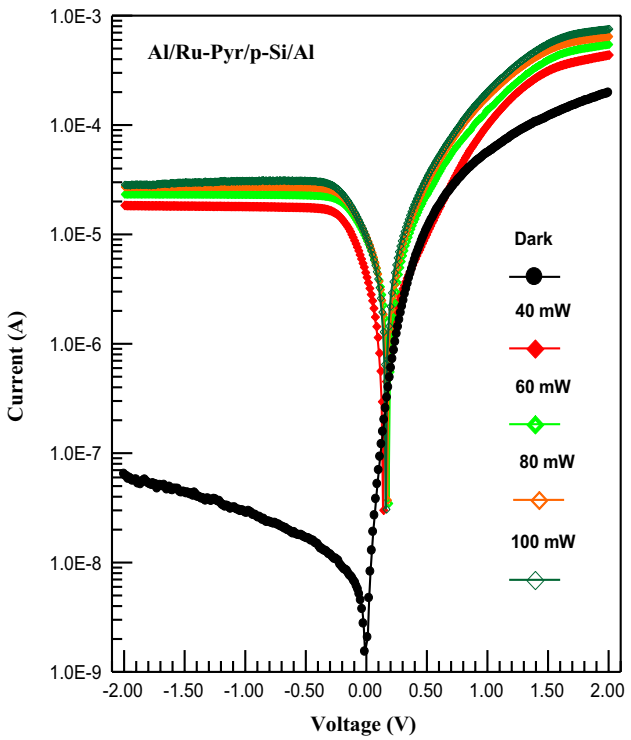

Fig. 6 The semi-logarithmic current–voltage (I–V) characteristics of the Al/Ru-Py/p-Si/Al device under various illumination intensities

Table 2 Electrical parameters derived from semi-logarithmic I–V characteristic for reference Al/p-Si/Al and Al/p-Si/Ru-Py/Al

Device structure	Ideality factor (n)	Barrier height (Φ_b) (eV)
Al/p-Si/Al	1.55	0.67
Al/p-Si/Ru-Py/Al	1.24	0.78

the devices were calculated as 1.55 and 1.24, respectively. In rectifier contacts, the deviation from the ideal state can be explained by the interface states, the load carriers that do not comply with the TE theory, the voltage drop in the interface layer, series resistance effects and the impurity rate at the interface (Monch 1999; Long, et al. 2014; Karataş, et al. 2007). The ability to control the barrier height of the device is one of the most important advantages of MS devices. This change in barrier height of the Al/Ru-Py/p-Si/Al device has shown that the barrier height can be controlled by covering the appropriate interface layers. Consequently, the increase in barrier height in the device structure has been attributed to the presence of Ru-Py complex at the interface (Baltakesmez et al. 2019; Aydogan et al. 2009; Caldiran et al. 2013a, b).

According to the I–V measurements, the basic diode parameter values were effected in a positive way by the Ru-Py complex layer. When I–V characteristics were examined at room temperature, it was concluded that Al/Ru-Py/p-Si/Al SBD had better rectifier properties and the ideality factor has decreased in dark conditions. However, the Al/Ru-Py/p-Si/Al device increased the current value under illuminated conditions and showed photodiode properties. The semi-logarithmic I–V characteristic of the device in 40, 60, 80 and 100 mW/cm^2 illumination intensities at room temperature, reverse and forward bias is given in Fig. 5. As can be seen in the plot, the device has been acting in harmony with TE by showing a rectifier feature in different illumination intensities. The difference in illumination in the semi-logarithmic I–V characteristic of the Al/Ru-Py/p-Si/Al SBD device is due to the photodiode behavior. Also, the graphs of the linear I–V characteristic in Fig. 7 in the dark and 100 mW/cm^2 illumination support the photodiode behavior (Vergeer, et al. 2006). As a result, the device obtained by coating the Ru-Py complex at the interface behaved in accordance with the literature (Koçyiğit et al. 2018; Sevgili et al. 2020; Cetinkaya et al. 2013) studies under different illumination conditions and is suitable for use as a reference device in photodiode applications.

Capacitance–voltage (C–V) characteristics

The reverse and forward bias voltage capacitance–voltage characteristics of the Al/Ru-Py/p-Si/Al device in the frequency range of 5-5000 kHz are given in Fig. 8. As can

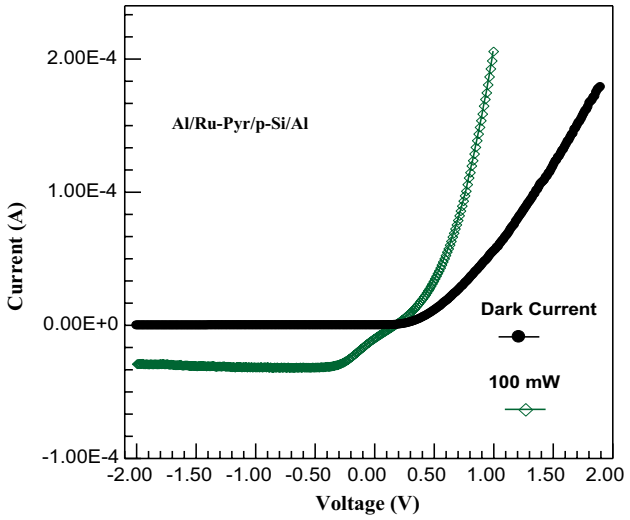

Fig. 7 The linear current–voltage (I–V) characteristics of the Al/Ru-Py/p-Si/Al device under 100 mW/cm^2 illumination

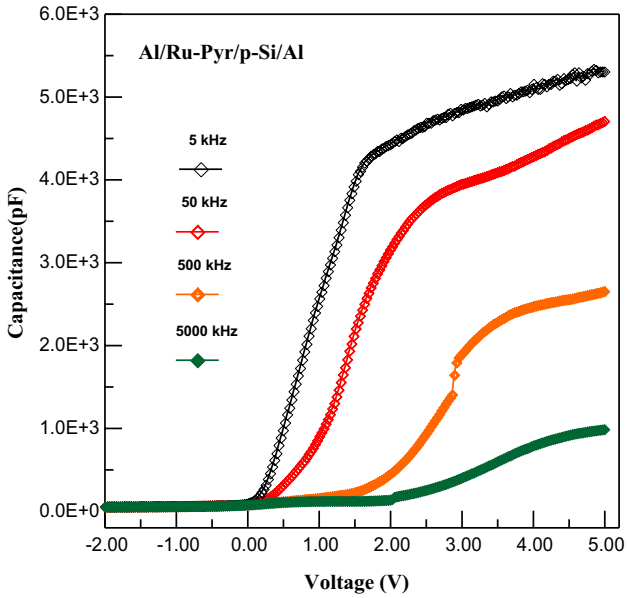

Fig. 8 The forward and the reverse bias C–V characteristics of the Al/Ru-Py/p-Si/Al device for various frequencies

be seen from the graphs, the capacitance decreased with increasing frequency. On the other hand, in the forward bias low-voltage region, the capacitance increased significantly; after 1.5 V the slope decreased. This is more evident at low frequencies. AC signals can be followed by interface states at low frequencies. Thus, a large capacitance is formed, which is defined as the additional space charge to the capacitance (Türüt et al. 2015; Werner et al. 1988; Arslan et al. 2010). Fusion potential (V_d), ionizing acceptor concentration (N_a), Fermi energy level (E_f) and barrier height ($\Phi_{b(C\text{-}V)}$) can be calculated from C–V measurements to obtain more detailed information about the depletion zone.

$$C^{-2} = \frac{2(V_0 + V)}{\varepsilon_s \varepsilon_0 q A^2 N_a} \tag{6}$$

where V_d is the diffusion potential obtained from the C^{-2}–V plot, ε_s, the dielectric constant of silicon (=11.8), the dielectric constant at 0 vacuum (= 8.85×10^{-14} F/m), the ionizing acceptor concentration of N_a. V_d and $\Phi_{b(C\text{-}V)}$ values are calculated using C–V measurements, respectively, as follows;

$$V_d = V_0 + \frac{kT}{q} \tag{7}$$

$$\Phi_{b(C\text{-}V)} = V_d + V_n \tag{8}$$

The difference between E_f and the base of the conductive band gives V_n.

$$E_f = kT \ln\left(\frac{N_a}{N_v}\right) \tag{9}$$

Here, N_v is the influential density states (=1.04×10^{19} cm^{-3} for Si). C–V graphs of the Al/Ru-Py/p-Si/Al SBD device depending on the frequency between 5 and 5000 kHz are given in Fig. 8.

In Fig. 9, the C^{-2}–V plot obtained from the reverse bias of the capacitance–voltage characteristic is seen. Table 3 shows the variation of V_d, N_a, E_f and $\Phi_{b(C\text{-}V)}$ parameters calculated using the C^{-2}–V plot according to frequency. The difference between Φ_b obtained from I–V measurements and Φ_b obtained from capacitance–voltage measurements is due to the nature of the measurement methods. The differences in barrier height can be attributed to the inhomogeneity in the interfacial layer and the distribution of interface carriers (Güllü et al. 2010).

Conclusions

The Ru-Py complex materials have been synthesized in high yield by reaction of $RuCl_3.H_2O$ with the pyridine ligands. The structural characterization of the Ru-Py complex has been evaluated by using NMR, IR, UV–Vis, fluorescence spectroscopy, HRMS and X-ray single-crystal diffraction techniques. It has been observed the Ru-Py complex performs blue wavelength optical absorption in the visible region. The synthesized Ru-Py complex materials to produce the Al/Ru-Py/p-Si/Al SBD structure was coated on p-type Si. The values of n and Φb of devices were calculated in semi-logarithmic current–voltage characteristics by the TE method. Ultimately, the Al/Ru-Py/p-Si/Al SBD showed

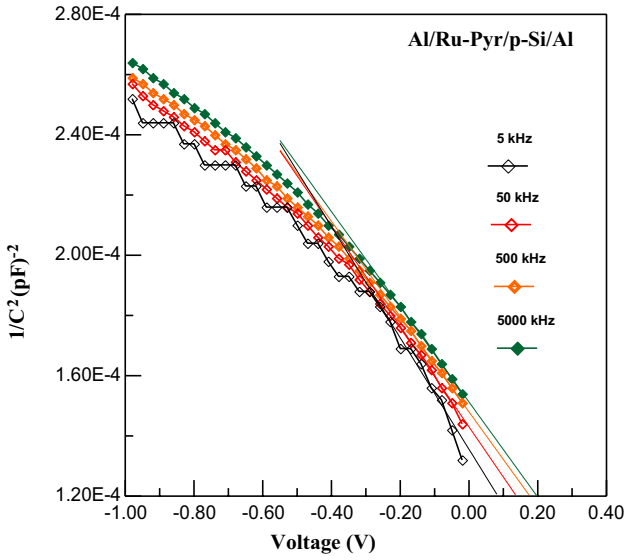

Fig. 9 Frequency-dependent 1/C2–V plots of Al/Ru-Py/p-Si/Al device in reverse bias voltage at room temperature

Table 3 Some electrical parameters of Al/Ru-Py/p-Si/Al device calculated using $1/C^2$–V plots

Frequency (kHz)	V_d (V)	N_a (cm^{-3})x10^{15}	E_f (eV)	$\Phi_{b(C\text{-}V)}$ (eV)
5	0.75	1.1	0.26	0.85
50	0.86	1.2	0.26	0.98
500	0.94	1.2	0.26	1.00
5000	0.96	1.2	0.26	1.01

good rectifying with the mean ideality factor of 1.24 and the barrier height of 0.78 eV. When the SBD obtained with Ru-Py complex and MS were compared, it was seen that the n value decreased and the Φ_b value increased with the Ru-Py complex effect. This change in device behavior is due to the reconstruction of the loads in the interface states with the Ru-Py complex effect, the serial resistance of the device and the interface polarization. Besides the barrier diode properties, it was concluded that Al/Ru-Py/p-Si/Al structure is a suitable alternative for photovoltaic applications with its light-dependent behavior. In addition, it was clearly seen that the capacitance–voltage characteristic of the device obtained with the Ru-Py complex changed depending on the frequency and the barrier height increased with the frequency.

Supplementary Material

Crystallographic data for the structural analysis have been deposited with the Cambridge Crystallographic Data Centre, CCDC No. 2052206. Copies of this information may be obtained free of charge from the Director, CCDC, 12 Union Road, Cambridge CB2 1EZ, UK (fax:+44-1223-336033; e-mail: deposit@ccdc.cam.ac.uk or www:http://www.ccdc.cam.ac.uk).

Supplementary Information The online version contains supplementary material available at https://doi.org/10.1007/s11696-021-01715-7.

Acknowledgements The author would like to thank Dr. Z. Çaldıran and Dr. I. Orak for their helps and Dr. O. Şahin for the precious discussion about X-ray results.

References

Ahmad Z, Sayyad MH (2009) Extraction of electronic parameters of Schottky diode based on an organic semiconductor methyl-red. Physica E 41:631–634. https://doi.org/10.1016/j.physe.2008.08.068

Alessio N, Balducci G, Calligaris M, Costa G, Attia WM, Mestroni G (1991) Synthesis, molecular structure, and chemical behavior of hydrogen trans-bis(dimethyl sulfoxide)tetrachlororuthenate(III) and mer-trichlorotris(dimethyl sulfoxide)ruthenium(III): the first fully characterized chloride-dimethyl sulfoxide-ruthenium(III) complexes. Inorg Chem 30:609–618. https://doi.org/10.1021/ic00004a005

Altındal S, Dokme I, Bulbul MM, Yalcin N, Serin T (2006) The role of the interface insulator layer and interface states on the current-transport mechanism of Schottky diodes in wide temperature range. Microelectron Eng 83:499–505. https://doi.org/10.1016/j.mee.2005.11.014

Arslan E, Safak Y, Altındal S, Kelekci O, Ozbay E (2010) Temperature dependent negative capacitance behavior in (Ni/Au)/AlGaN/AlN/GaN heterostructures. J Non-Cryst Solids 356:1006–1011. https://doi.org/10.1016/j.jnoncrysol.2010.01.024

Aydogan S, Saglam M, Türüt A, Onganer Y (2009) Series resistance determination of Au/Polypyrrole/p-Si/Al structure by current-voltage measurements at low temperatures. Mat Sci Eng C-Bio S 29:1486–1490. https://doi.org/10.1016/j.msec.2008.12.006

Baltakesmez A, Taşer A, Kudas Z, Guzeldir B, Ekinci D, Saglam M (2019) Barrier height modification of n-InP using a silver nanoparticles loaded graphene oxide as an interlayer in a wide temperature range. J Electron Mater 48:3169–3182. https://doi.org/10.1007/s11664-019-07088-8

Batista AA, Onofre SA, Queiroz SL, Oliva G, Fontes MRM, Nascimento OR (1997) Synthesis, characterization and molecular structures of the pyridinium trans-bis(pyridine) tetrachlororuthenate(III) and pyridinium trans-(carbonyl)(pyridine)tetrachlororuthenate(III). J Brazil Chem Soc 8:641–647. https://doi.org/10.1590/S0103-50531997000600001

Benavides PA, Matias TA, Araki K (2017) Unexpected lability of the [RuIII(phtpy)Cl_3]complex. Dalton Trans 46:15567–15572. https://doi.org/10.1039/c7dt03658b

Białek MJ, Latos-Grażyński L (2016) Palladium(II), ruthenium(II), and ruthenium(III) complexes of 23-thiaazuliporphyrin: the case of coordination-induced contraction. Inorg Chem 55:1758–1769. https://doi.org/10.1021/acs.inorgchem.5b02684

Çaldıran Z (2020) Fabrication of Schottky barrier diodes with the lithium fluoride interface layer and electrical characterization in a wide temperature range. J Alloy Compd. https://doi.org/10.1016/j.jallcom.2019.152601

Çaldıran Z, Deniz AR, Aydogan S, Yesildag A, Ekinci D (2013) The barrier height enhancement of the Au/n-Si/Al Schottky barrier diode by electrochemically formed an organic Anthracene layer

on n-Si. Superlattice Microst 56:45–54. https://doi.org/10.1016/j.spmi.2012.12.004
Çaldıran Z, Deniz AR, Sahin Y, Metin O, Meral K, Aydogan S (2013) The electrical characteristics of the Fe3O4/Si junctions. J Alloy Compd 552:437–442. https://doi.org/10.1016/j.jallcom.2012.11.079
Çetinkaya HG, Tecimer H, Uslu H, Altındal S (2013) Photovoltaic characteristics of Au/PVA (Bi-doped)/n-Si Schottky barrier diodes (SBDs) at various temperatures. Curr Appl Phys 13:1150–1156. https://doi.org/10.1016/j.cap.2013.03.010
Chen Z, Wang JJ, Ren YH, Yu CL, Shum K (2012) Schottky solar cells based on CsSnI3 thin-films. Appl Phys Lett doi. https://doi.org/10.1063/1.4748888
Chmielewski PJ, Latos-Grazynski L, Pacholska E (1994) Lowvalent nickel thiaporphyrins nuclear magnetic resonance and electron paramagnetic resonance studies. Inorg Chem 33:1992–1999. https://doi.org/10.1021/ic00087a040
Coşkun FM, Polat O, Coşkun M, Türüt A, Caglar M, Durmus Z, Efeoglu H (2019) Temperature dependent current transport mechanism in osmium-doped perovskite yttrium manganite-based heterojunctions. J Appl Phys. https://doi.org/10.1063/1.5094129
Deniz AR, Çaldıran Z, Biber M, Incekara U, Aydogan S (2018) Investigation of electrical properties of Ni/Crystal Violet (C25H30CIN3)/n-Si/Al diode as a function of temperature. J Alloy Compd 763:622–628. https://doi.org/10.1016/j.jallcom.2018.05.295
Di Bartolomeo A, Grillo A, Urban F, Iemmo L, Giubileo F, Luongo G, Amato G, Croin L, Sun LF, Liang SJ, Ang LK (2018) Asymmetric schottky contacts in bilayer MoS2 field effect transistors. Adv Funct Mater. https://doi.org/10.1002/adfm.201800657
Djeghlouf A, Hamri D, Teffahi A, Saidane A, Al Mashary FS, Al Huwayz MM, Henini M, Orak I, Albadri AM, Alyamani AY (2019) Effect of indium doping on the electrical and structural properties of TiO2 thin films used in MOS devices. J Alloy Compd 775:202–213. https://doi.org/10.1016/j.jallcom.2018.10.048
Dragonetti C, Valore A, Colombo A, Magni M, Mussini P, Roberto D, Ugo R, Valsecchi A, Trifiletti V, Manfredi N, Abbotto A (2013) Ruthenium oxyquinolate complexes for dye-sensitized solar cells. Inorg Chim Acta 405:98–104. https://doi.org/10.1016/j.ica.2013.05.006
Ejderha K, Zengin A, Orak I, Taşyürek B, Kilinc T, Türüt A (2011) Dependence of characteristic diode parameters on sample temperature in Ni/epitaxy n-Si contacts. Mat Sci Semicon Proc 14:5–12. https://doi.org/10.1016/j.mssp.2010.12.010
Farag AAM, Gunduz B, Yakuphanoglu F, Farooq WA (2010) Controlling of electrical characteristics of Al/p-Si Schottky diode by tris(8-hydroxyquinolinato) aluminum organic film. Synthet Met 160:2559–2563. https://doi.org/10.1016/j.synthmet.2010.10.005
Farrugia LJ (1999) WinGX suite for small-molecule single-crystal crystallography. J Appl Crystallogr 32:837–838. https://doi.org/10.1107/S0021889899006020
Gao F, Zhang DK, Wang JY, Sun HB, Yin Y, Sheng Y, Yan SC, Yan B, Sui CH, Zheng YD, Shi Y, Liu JL (2016) Ultraviolet electroluminescence from Au-ZnO nanowire Schottky type light-emitting diodes. Appl Phys Lett. https://doi.org/10.1063/1.4954758
Güllü O, Kilicoglu T, Türüt A (2010) Electronic properties of the metal/organic interlayer/inorganic semiconductor sandwich device. J Phys Chem Solids 71:351–356. https://doi.org/10.1016/j.jpcs.2009.12.089
Güllü O, Türüt A (2015) Electronic parameters of MIS Schottky diodes with DNA biopolymer interlayer. Mater Sci-Poland 33:593–600. https://doi.org/10.1515/msp-2015-0089
Gupta RK, Singh RA (2004) Schottky diode based on composite organic semiconductors. Mat Sci Semicon Proc 7:83–87. https://doi.org/10.1016/j.mssp.2004.05.002
Izaki M, Shinagawa T, Mizuno KT, Ida Y, Inaba M, Tasaka A (2007) Electrochemically constructed p-Cu2O/n-ZnO heterojunction diode for photovoltaic device. J Phys D Appl Phys 40:3326–3329. https://doi.org/10.1088/0022-3727/40/11/010
Juris A, Balzani V, Barigelletti F, Campagna S, Belser P, Vonzelewsky A (1988) Ru(II) polypyridine complexes: photophysics, photochemistry, eletrochemistry, and chemiluminescence. Coordin Chem Rev 84:85–277. https://doi.org/10.1016/0010-8545(88)80032-8
Kacus H, Deniz AR, Çaldıran Z, Aydogan S, Yesildag A, Ekinci D (2014) The analysis of the current-voltage characteristics of the high barrier Au/Anthracene/n-Si MIS devices at low temperatures. Mater Chem Phys 143:545–551. https://doi.org/10.1016/j.matchemphys.2013.09.030
Kar MK, Singh MK, Lal RA (2017) Synthesis and spectral studies on monometallic ruthenium (III) complexes of N-(2-hydroxysalicyliden-1-yl)methylenebenzoylhydrazide. Arabian J Chem 10:S76–S80. https://doi.org/10.1016/j.arabjc.2012.05.007
Karabulut A, Türüt A, Karataş S (2018) The electrical and dielectric properties of the Au/Ti/Hf02/n-GaAs structures. J Mol Struct 1157:513–518. https://doi.org/10.1016/j.molstruc.2017.12.087
Karataş S, Altındal S, Türüt A, Cakar M (2007) Electrical transport characteristics of Sn/p-Si schottky contacts revealed from I-V-T and C-V-T measurements. Physica B 392:43–50. https://doi.org/10.1016/j.physb.2006.10.039
Koçyiğit A, Karteri I, Orak I, Urus S, Caylar M (2018) The structural and electrical characterization of Al/GO-SiO2/p-Si photodiode. Physica E 103:452–458. https://doi.org/10.1016/j.physe.2018.06.006
Koçyiğit A, Orak I, Çaldıran Z, Türüt A (2017) Current-voltage characteristics of Au/ZnO/n-Si device in a wide range temperature. J Mater Sci-Mater El 28:17177–17184. https://doi.org/10.1007/s10854-017-7646-3
Kroghjespersen K, Schugar HJ (1984) Detailed correlations between the ligand-to-metal charge-transfer (LMCT) spectra of copper(ii) and ruthenium(iii) imidazoles and imidazolates—electronic-structures of carbon-bound ruthenium(iii) Imidazoles and Imidazolates. Inorg Chem 23:4390–4393. https://doi.org/10.1021/ic00193a060
Lakshmanan L, Shivaprakash NC, Sindhu S (2018) Orange fluorescent Ru(III) complexes based on 4′-aryl substituted 2,2′:6′,2″-terpyridine for OLEDs application. J Fluoresc 28:173–182. https://doi.org/10.1007/s10895-017-2180-5
Latos-Grazynski L, Lisowski J, Olmstead MM, Balch AL (1989) Five-coordinate complexes of 21-thiaporphyrin. Preparations, spectra, and structures of iron (II), nickel (II), and copper (II) complexes. Inorg Chem 28:3328–3331. https://doi.org/10.1021/ic00316a015
Long W, Li Y, Tung RT (2014) Schottky barrier height systematics studied by partisan interlayer. Thin Solid Films 557:254–257. https://doi.org/10.1016/j.tsf.2013.10.075
Manoharan PT, Mehrotra PK, Taquikha MM, Andal RK (1973) Optical and magnetic properties and geometry of some D5 ruthenium complexes. Inorg Chem 12:2753–2757. https://doi.org/10.1021/ic50130a003
Metin O, Aydogan S, Meral K (2014) A new route for the synthesis of graphene oxide-Fe3O4 (GO-Fe3O4) nanocomposites and their Schottky diode applications. J Alloy Compd 585:681–688. https://doi.org/10.1016/j.jallcom.2013.09.159
Mohite SS, Patil-Deshmukh AB, Chavan SS (2020) Ru(III)-pseudohalide complexes with alkynyl functionalized salicylaldimine ligand and heterocyclic coligand: Synthesis, characterization, electrochemical and luminescence properties. Inorganica Chimica Acta. https://doi.org/10.1016/j.ica.2020.119586
Monch W (1999) Barrier heights of real Schottky contacts explained by metal-induced gap states and lateral inhomogeneities. J Vac Sci Technol B 17:1867–1876. https://doi.org/10.1116/1.590839

Orak I, Koçyiğit A, Türüt A (2017) The surface morphology properties and respond illumination impact of ZnO/n-Si photodiode by prepared atomic layer deposition technique. J Alloy Compd 691:873–879. https://doi.org/10.1016/j.jallcom.2016.08.295

Orhan Z, Cinan E, Caldiran Z, Kurucu Y, Das E (2020) Synthesis of CuO-graphene nanocomposite material and the effect of gamma radiation on CuO-graphene/p-Si junction diode. J Mater Sci-Mater El 31:12715–12724. https://doi.org/10.1007/s10854-020-03823-8

Park WI, Yi GC, Kim JW, Park SM (2003) Schottky nanocontacts on ZnO nanorod arrays. Appl Phys Lett 82:4358–4360. https://doi.org/10.1063/1.1584089

Petronella F, Fanizza E, Mascolo G, Locaputo V, Bertinetti L, Martra G, Coluccia S, Agostiano A, Curri ML, Comparelli R (2011) Photocatalytic activity of nanocomposite catalyst films based on nanocrystalline metal/semiconductors. J Phys Chem C 115:12033–12040. https://doi.org/10.1021/jp201098t

Punetha D, Pandey SK (2019) Ultrasensitive NH3 gas sensor based on Au/ZnO/n-Si heterojunction schottky diode. Ieee T Electron Dev 66:3560–3567. https://doi.org/10.1109/TED.2019.2921990

Ravikiran L, Radhakrishnan K, Dharmarasu N, Agrawal M, Wang ZL, Bruno A, Soci C, Tng LH, Siong AK (2016) Responsivity drop due to conductance modulation in GaN metal-semiconductor-metal Schottky based UV photodetectors on Si(111). Semicond Sci Tech. https://doi.org/10.1088/0268-1242/31/9/095003

Reddy VR, Choi CJ (2020) Microstructural and interface properties of Au/SrTiO3 (STO)/n-GaN heterojunction with an e-beam evaporated high-k STO interlayer. J Alloy Compd. https://doi.org/10.1016/j.jallcom.2020.153775

Sauvage JP, Collin JP, Chambron JC et al (1994) Ruthenium(II) and Osmium(II) Bis(terpyridine) complexes in covalently-linked multicomponent systems: synthesis, electrochemical behavior, absorption spectra, and photochemical and photophysical properties. Chem Rev 94:993–1019. https://doi.org/10.1021/cr00028a006

Sevgili O, Canli S, Akman F, Orak I, Karabulut A, Yıldırım N (2020) Characterization of aluminum 8-hydroxyquinoline microbelts and microdots, and photodiode applications. J Phys Chem Solids. https://doi.org/10.1016/j.jpcs.2019.109128

Sheldrick GM (2008) A short history of SHELX. Acta Crystallogr A 64:112–122. https://doi.org/10.1107/S0108767307043930

Sheldrick GM (2015) Crystal structure refinement with SHELXL. Acta Crystallogr C 71:3–8. https://doi.org/10.1107/S2053229614024218

Siek TJ, Osiewicz RJ (1975) Identification of drugs and other toxic compounds from their ultraviolet spectra. Part II: Ultraviolet absorption properties of thirteen structural groups. J Forensic Sci 20:18–37 (**PMID: 1117267**)

Taqui Khan MM, Chatterjee D, Hussain A, Moiz MA (1993) Synthesis and characteristics of mixed ligand Ru(II1) complexes with EDTA-polypyridyl, and Pt/TiOz/RuOz semiconductor particulate system modified by the complexes. J Photochem Photobiul A Chum 76:97–101. https://doi.org/10.1016/1010-6030(93)80179-D

Taşer A, Guzeldir B, Saglam M (2017) The stability of electrical characteristics of Ti/n-Si/Ag, Ti/n-Si/Cu and Ti/nSi/AgCu diodes prepared under the same conditions with respect to increasing aging time. Mat Sci Semicon Proc 68:186–192. https://doi.org/10.1016/j.mssp.2017.06.014

Taşyürek LB, Aydogan S, Sevim M, Çaldıran Z (2020) Temperature dependent electronic transport properties of heterojunctions formed between perovskite SrTiO(3)nanocubes and silicon. J Mater Sci-Mater El 31:20833–20846. https://doi.org/10.1007/s10854-020-04597-9

Taşyürek LB, Sevim M, Çaldıran Z, Aydogan S, Metin O (2018) The synthesis of SrTiO3 nanocubes and the analysis of nearly ideal diode application of Ni/SrTiO3 nanocubes/n-Si heterojunctions. Mater Res Express. https://doi.org/10.1088/2053-1591/aaa745

Tuğluoğlu N, Karadeniz S, Altındal S (2005) Effect of series resistance on the performance of silicon Schottky diode in the presence of tin oxide layer. Appl Surf Sci 239:481–489. https://doi.org/10.1016/j.apsusc.2004.06.015

Tung RT (2001) Recent advances in Schottky barrier concepts. Mat Sci Eng R 35:1–138. https://doi.org/10.1016/S0927-796X(01)00037-7

Türüt A, Karabulut A, Ejderha K, Biyikli N (2015) Capacitance-conductance-current-voltage characteristics of atomic layer deposited Au/Ti/Al2O3/n-GaAs MIS structures. Mat Sci Semicon Proc 39:400–407. https://doi.org/10.1016/j.mssp.2015.05.025

Umamahesh B, Karthikeyan NS, Sathiyanarayanan KI, Malicka JM, Cocchi M (2016) Tetrazole iridium(III) complexes as a class of phosphorescent emitters for high-efficiency OLEDs. J Mater Chem C 4:10053–10060. https://doi.org/10.1039/C6TC03217F

Vergeer FW, Chen XD, Lafolet F, De Cola L, Fuchs H, Chi LF (2006) Ultrathin luminescent films of rigid dinuclear ruthenium(II) tris-bipyridine complexes. Adv Funct Mater 16:625–632. https://doi.org/10.1002/adfm.200500446

Webb MI, Wu B, Jang T, Chard RA, Wong EWY, Wong MQ, Yapp DTT, Walsby CJ (2013) Increasing the bioavailability of Ru-III anticancer complexes through hydrophobic albumin interactions. Chem-Eur J 19:17031–17042. https://doi.org/10.1002/chem.201302671

Werner J, Levi AFJ, Tung RT, Anzlowar M, Pinto M (1988) Origin of the excess capacitance at intimate schottky contacts. Phys Rev Lett 60:53–56. https://doi.org/10.1103/PhysRevLett.60.53

Yılmaz M, Cirak BB, Aydogan S, Grilli ML, Biber M (2018) Facile electrochemical-assisted synthesis of TiO2 nanotubes and their role in Schottky barrier diode applications. Superlatt Microst 113:310–318. https://doi.org/10.1016/j.spmi.2017.11.009

Zhang J, Chu BWK, Zhu N, Yam VWW (2007) Synthesis, characterization, langmuir–blodgett film-forming property, and second-order nonlinear optical study of Rhenium(I) and Ruthenium(II) diimine complexes. Organometallics 26:5423–5429. https://doi.org/10.1021/om070030b